IOP PUBLISHING JOURNAL OF MICROMECHANICS AND MICROENGINEERING

J. Micromech. Microeng. 18 (2008) 035033 (9pp) doi:10.1088/0960-1317/18/3/035033

Integration of out-of-plane silicon dioxide microtubes, silicon microprobes and on-chip NMOSFETs by selective vapor–liquid–solid growth

Kuniharu Takei[1,4], Takahiro Kawashima[1,2], Takeshi Kawano[1,3], Hidekuni Takao[1,2,3], Kazuaki Sawada[1,2,3] and Makoto Ishida[1,2,3]

[1] Toyohashi University of Technology, Department of Electrical and Electronic Engineering, 1–1 Hibarigaoka, Tempaku-cho, Toyohashi, Aichi 441-8580, Japan
[2] Toyohashi University of Technology, Intelligent Sensing System Research Center, Japan
[3] Japan Science and Technology Agency—CREST, Kawaguchi, Saitama 332-0012, Japan
[4] Research Fellow of the Japan Society for the Promotion of Science, 8, Ichiban-cho, Chiyoda-ku, Tokyo 102-8472, Japan

E-mail: takei@dev.eee.tut.ac.jp

Received 4 December 2007, in final form 21 January 2008
Published 13 February 2008
Online at stacks.iop.org/JMM/18/035033

Abstract

Three-dimensional microtubes and microprobes with MOSFET circuits are integrated for use in chemical and electrical neural interface applications with microelectronics. We propose a vapor–liquid–solid (VLS) method to realize both the microtubes and microprobes, which are 2 μm and 3.6 μm in diameter, respectively, and can be fabricated after the on-chip MOSFET processes. The on-chip NMOSFET shows electrical characteristics with a threshold voltage of 1.2 V and a subthreshold swing of 145 mV decade^{-1}, confirming that subsequent fabrications of the tube and probe are compatible with the inclusion of the on-chip circuits. The prototype oxide tube, which has 2.7 μm inner diameter and 29 μm height, has a flow rate of 550 nl min^{-1} with an external pump pressure of 33.5 kPa. The impedance of the on-chip Si probe, which has 2 μm diameter and 30 μm height, measured at 1 kHz in a saline environment is 2 MΩ. Insertion into a gelatin membrane confirms that both the tube and the probe show sufficient penetration capabilities.

(Some figures in this article are in colour only in the electronic version)

1. Introduction

Although a significant portion of brain function has been investigated [1], details of the signal networks of neurons require further studies because they are very complex and there are numerous hurdles that must be overcome to record local neural signals [2–6]. To resolve these issues, many institutions have proposed a plethora of electrical microelectrodes [5–8].

Moreover, drug delivery systems also require neural behaviors to be studied because neurons act with biochemical reactions [9–12]. Therefore, chemical reactions in tissues must be observed while simultaneously recording neural signals. If drug delivery systems and the electrical recording systems are incorporated in the same substrate, then this would aid in the understanding of these complex neural networks [13–17]. In addition, the proposed device, which has both a drug delivery system and a recording system, may be applicable as an interface device between the brain and organs in paralyzed patients, and may aid in the patient regaining functions. For example, drugs can automatically be delivered to a particular area through a microtube to cure the tissue while detecting abnormal signals from neurons with an electrical probe electrode. Researchers at Brown University have already implanted a microelectrode array with wires

 © 2008 IOP Publishing Ltd Printed in the UK

into a human brain [20]. According to their paper, a male with a transected spinal cord, which resulted in complete quadriplegia, has regained brain/hand coordination by means of a cursor on a PC screen via a silicon (Si) microelectrode array implanted into the primary motor cortex (MI) arm area. If devices with signal processing circuits can be fabricated, then interface devices should be more attractive for human use.

Si-based fabrication techniques can realize microprobe electrode arrays [19, 20] and microtube arrays for drug delivery [9–12, 16–18]. In addition, both a probe and tube on the same substrate [13–15] have been realized by utilizing deep reactive ion etching (DRIE) and wet etching as well as dicing techniques. Recent papers have reported polymeric material based drug delivery systems, which are biocompatible devices [15–18]. However, the fabrication techniques must further be improved in order to reduce the tube/probe size to ensure the device is minimally invasive and causes little damage of the neurons/tissues *in vivo* until reaching the target neurons.

We have proposed selective vapor–liquid–solid (VLS) growth of Si to fabricate microprobe electrode arrays [21–24] and microtube arrays [25]. These Si probes can be integrated with on-chip MOSFETs by subsequent VLS growth, which allows on-chip signal processors such as signal amplifications, multiplexers as well as wireless interface systems to be incorporated [19, 26, 27].

In this paper, we present fabrication techniques to integrate both a silicon dioxide (SiO_2) microtube and Si microprobe with on-chip MOSFETs for use as a simultaneous extracellular drug delivery system and an electrical recording system to document activities of the retina, peripheral nerves, brain, etc. Moreover, we discuss the MOSFET characteristics after the fabrication processes of the VLS-Si probe and the SiO_2 tube, the electrical properties of the probe and liquid flow characteristics of the tube. The mechanical robustness of the SiO_2 tube and Si probe are analyzed by both finite element method (FEM) and experimental insertion into a gelatin.

2. Preparation of an on-chip NMOSFET

2.1. Interconnection

In our previous work [23], a WSi_2 material was used as the interconnection. However, WSi_2 on insulating SiO_2 does not withstand high-temperature processes due to poor adhesion between the WSi_2 interconnection and the SiO_2 layer. The results of poor adhesion indicate the low yield of the device, but stable interconnection materials and structures with good adhesion are very important if the device is used to integrate signal processing circuits.

To realize the integration of a SiO_2 tube and Si probe with MOSFETs, a suitable interconnection material, other than Al, is necessary. To investigate the interconnection material, W, WSi_2, TiN and Ti were formed over a SiO_2 layer, the materials were then patterned and covered with another SiO_2 layer to protect from additional thermal diffusion with phosphorous. After SiO_2 formation, phosphorus diffusion with O_2, N_2 and $POCl_3$ at 900 °C for 1 h and 1.5 h was performed.

2.2. Hydrogen annealing for NMOSFETs

The electrical characteristics of on-chip MOSFETs were measured with a semiconductor parameter analyzer (4156C, Agilent Technologies, USA). According to our previous work, hydrogen annealing of MOSFET on Si(1 1 1) is an effective process to terminate dangling bonds and to decrease interface states [28]. In this study, the electrical characteristics were compared before and after the hydrogen annealing when the VLS growth process and fabrication process of the tube structures had been applied. We used an annealing ambient of 4% hydrogen in nitrogen, at 460 °C with an annealing time of 3 h.

3. Fabrication processes

Figure 1 illustrates the fabrication techniques of microprobes and microtubes, which required two steps after the on-chip MOSFET fabrication. The processes began with a Si substrate and on-chip circuits fabricated by an in-house-CMOS process (5 μm process rule, Electron Device Research Center (EDRC) at Toyohashi University of Technology). In the first step, the Si microprobes were fabricated by selective VLS growth, while in the second step, some of the Si microprobes were formed as SiO_2 microtubes. We initially prepared the on-chip MOSFETs on a 350 μm thick n-type Si (1 1 1) substrate. The Si probes were designed in the drain region of the NMOSFETs in a site selector and the SiO_2 tubes were placed 200 μm from the probe. Before the probe fabrication, the Si substrate was etched from the backside with a depth of about 300 μm by deep RIE in order to form flow channels for the tubes (figure 1(*a*)).

3.1. Si microprobe

After the MOSFET processes (figure 1(*a*)), a Si probe array was fabricated by VLS growth [21, 22]. A 160 nm thick Au film was formed selectively as the catalyst (figure 1(*b*)). VLS growth was carried out in a gas-source molecular-beam-epitaxy (GS-MBE) chamber with Si_2H_6 gas at 6.7×10^{-3} Pa, while the substrate was heated at 680 °C for 25 min (figure 1(*c*)). It should be noted that the substrate was annealed at 680 °C for a few minutes before the VLS growth so that an Au–Si alloy is formed between the Au film and the Si substrate. The fabricated Si probe exhibited electrical high-resistivity characteristics due to the intrinsic Si growth with the Si_2H_6 gas. Phosphorous thermal diffusion in a furnace at 900 °C for 1 h with N_2, O_2 and $POCl_3$ gases can reduce these resistivity characteristics (figure 1(*d*)) [22].

3.2. SiO_2 microtube

After the probe processes, a 450 nm thick SiO_2 layer was deposited over the substrate by plasma enhanced chemical vapor deposition (PECVD) to form the tube wall (figure 1(*e*)). The deposition parameters were SiH_4 gas of 65 sccm, N_2O gas of 120 sccm, deposition pressure of 67 Pa, RF power of 30 W and temperature of 350 °C. The deposition rate of

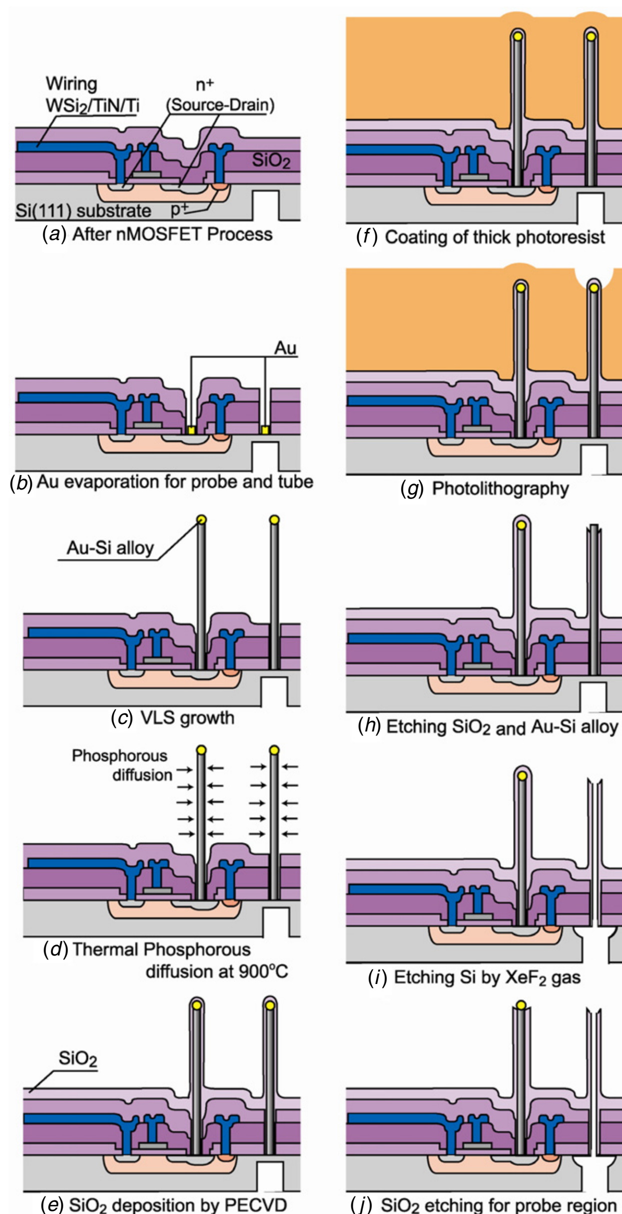

Figure 1. Process sequence for the probe and tube arrays integrated with NMOSFETs.

SiO_2 over the probe was 34.6 nm min^{-1}. A focused ion beam (FIB) system (SMI3200TS, SII NanoTechnology Inc., Japan) was used to prepare a cross-sectional view of the SiO_2-coated probe. Figure 2 shows a typical cross-sectional SEM view of the SiO_2/Si probe with a very smooth SiO_2 surface and the SiO_2–Si probe interface. Further, photolithography was conducted to etch the SiO_2 layer from the tip of the probe. The photoresist used here was PMER, which was a thick and positive type resist (P-LA900PM, Tokyo Ohka Kogyo Co., Ltd, Japan). After the photoresist coating, only the tube region was exposed and etched the SiO_2 portion by buffered hydrofluoric acid (BHF) (figure 1(*f*)–(*h*)). The exposed Au–Si alloy was removed by dipping the substrate into aqua regia (figure 1(*h*)). Subsequently, the inner Si body was etched using

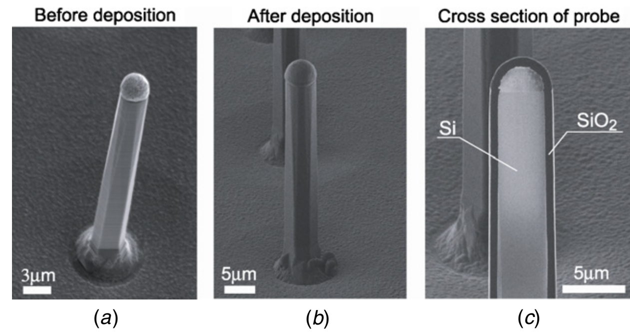

Figure 2. SEM and FIB images of a Si microprobe before and after SiO_2 deposition: (*a*) SEM image of the probe before deposition (tilt: 45°), (*b*) FIB image after deposition (tilt: 60°) and (*c*) cross-sectional image of the probe formed by FIB (tilt: 60°).

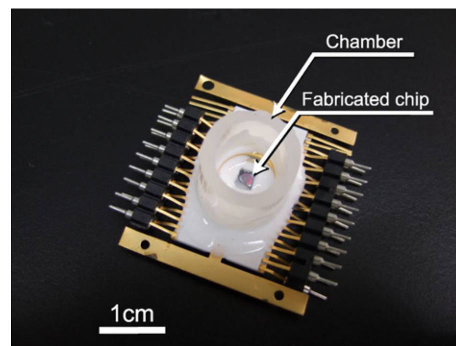

Figure 3. Photograph of a packaged device for electrical measurement of Si microprobes.

XeF_2 gas (figure 1(*i*)), resulting in a SiO_2 tube connected to the flow channel at the backside of the substrate. To complete the device, SiO_2 at the tip of the probe electrode was removed with BHF to permit the probe to be used in electrical recordings (figure 1(*j*)).

4. Experimental setup and methods

4.1. Impedance measurement and signal recording

To measure the impedance of the probe electrode in a saline solution, the fabricated device was mounted on a ceramic package using the chamber preparation shown in figure 3. Au wire bonding, which was used for the electrical connections between the device and the package, was covered with silicon glue to protect the device from the saline solution. The electrolyte, 0.9% NaCl saline solution, was then placed into the chamber as shown in figure 3. A standard reference electrode of a chlorinated silver wire (Ag–AgCl) was also placed into the saline solution, and test sinusoidal waves with 100 $mV_{p\text{-}p}$ amplitude and frequency range of 40 Hz to 10 MHz were applied. The impedance of each silicon probe was measured using an impedance analyzer (Agilent Technology, 4294A, USA).

In addition, the signal output through the microprobe was investigated by the input of sinusoidal waves, as illustrated in figure 4. Sinusoidal waves with a 1 kHz frequency and

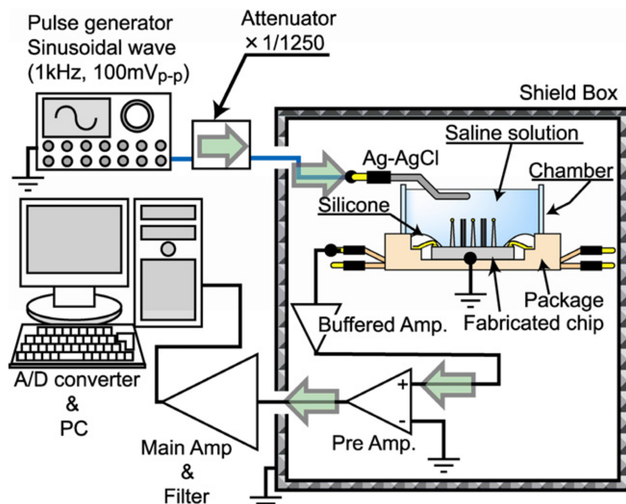

Figure 4. Schematic image of the measurement system used to observe the output/input signal through the microprobes in a saline solution.

100 mV_{p-p} amplitude were generated using a function generator (Agilent Technology, 33220A, USA), and then attenuated to make the amplitude around 80 μV_{p-p}, which is similar to the amplitude of extracellular neural signals. The output signals were amplified by a buffered amplifier, a pre-amplifier and a main amplifier (gain: 50000, AB-611J, Nihon Koden, Japan). Moreover, the output signals passed through a band-pass filter (band-pass: 500 Hz–3 kHz, EW-610J, Nihon Koden, Japan) and a direct amplifier (gain: 10, AD-610J, Nihon Koden, Japan). The output signals via the microprobe were digitized at 10 MS s^{-1} with a 12-bit AD converter (NI PCI-6115, National Instruments, USA).

4.2. *Liquid flow characteristics of the microtube*

Depending on the flow pressure, it is important to measure the liquid flow properties through the tube. Figure 5 shows the measurement system, which consists of a syringe pump (Model 11 PicoPlus, Harvard, USA), a precise flow meter (SLG1430, Sensirion, Switzerland) and a pressure sensor (MM series, Honeywell, USA). The experimental measurement was performed with a deionized (DI) water flow rate from 100 nl min^{-1} to 1500 nl min^{-1}, which was achieved using the syringe pump.

4.3. *Mechanical properties of the probe and the tube*

Both the tube and probe must be mechanically robust during penetration into tissues such as the brain, peripheral nerves, etc. If the mechanical properties are understood, then it is possible to estimate the penetration capability of both the tube and the probe. To observe the bending properties, first the bending displacement of tube/probe can be observed with a 5 μm diameter tungsten needle, which is used to make contact with the tube/probe tip. Then, a tungsten needle can be manipulated with a submicron spatial resolution (SM3.25, MARZHAUSER, Germany) by a manipulator system. In our

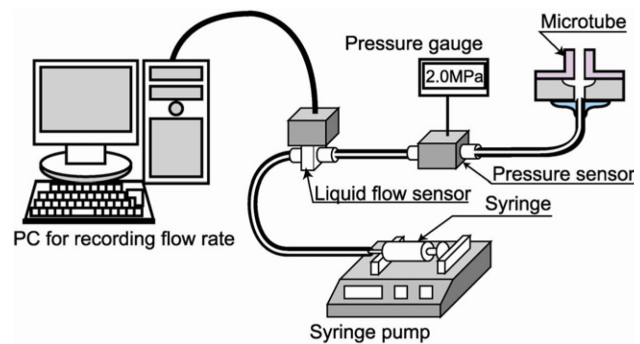

Figure 5. Schematic image of a fluidic characterization system.

experiment, the tube had a measured inner diameter of 3 μm and an outer diameter of 4 μm as well as a tube length of 40 μm. On the other hand, the probe had a 3 μm diameter and a length of 42 μm.

To confirm the penetration capability of the tube and probe array, penetration tests were carried out with a gelatin membrane *in lieu* of a tissue. The hardness of the gelatin was similar to the cardiac muscle of a pig. The device was a 5×5 array with alternating tubes and probes with 40 μm gaps. The gelatin was set up on the manipulator system. The fabricated device was fixed onto the stage of a microscope, and the gelatin was moved by the manipulator, which allowed the tube and probe to penetrate until the surface of the gelatin reached the surface of the device substrate.

5. Results and discussion

5.1. *Reliability of interconnection*

Figure 6 and table 1 show the results of the interconnections after annealing at 900 °C in a phosphorous gas ambient. The results indicate that WSi_2/TiN/Ti, WSi_2/TiN/Ti/poly-Si and Ti/TiN all exhibit good adhesion after the initial annealing for 1 h (data not shown), but a subsequent annealing for 30 min decreases the adhesion of the Ti/TiN interconnections. However, additional processing such as ion implantation was necessary for the WSi_2/TiN/Ti/poly-Si structure to reduce the resistance of the poly-Si. Consequently, the WSi_2/TiN/Ti on SiO_2/Si(1 1 1) is a reliable interconnection for use in subsequent high-temperature processes, including phosphorous diffusion at 900 °C.

5.2. *Tubes and probes with on-chip MOSFETs*

Figure 7(*a*) shows a photograph of the fabricate device, which consists of a 5×5 SiO_2 tube and Si probe array, and on-chip MOSFET circuits. Figure 7(*b*) depicts a SEM image of a Si microprobe fabricated at the drain region of the MOSFET. Figures 7(*c*) and (*d*) show an image of a SiO_2 microtube and a cross-sectional image of the tube, respectively. The image indicates that XeF_2 gas completely removed the inner Si. The SiO_2 microtubes were 29 μm long with inner and outer diameters of 2.7 μm and 3.6 μm, respectively. The Si microprobes were 30 μm long and 2 μm in diameter. A 0.45 μm uniformly thick SiO_2 layer was observed.

Table 1. Compatible interconnection structures for high-temperature processes.

	On SiO_2			On poly Si/SiO_2		
	W/TiN/Ti	Ti/TiN	WSi_2/TiN/Ti	W/TiN/Ti	Ti/TiN	WSi_2/TiN/Ti
Thickness (Å)	3500/400/600	3600/400	2700/500/900	3500/400/600	3600/400	2700/500/900
Adhesion after 1st anneal for 60 min	Bad	Very good	Very good	Very Bad	Good	Very good
Adhesion after 2nd anneal for 30 min		Good	Very good		Bad	Very good

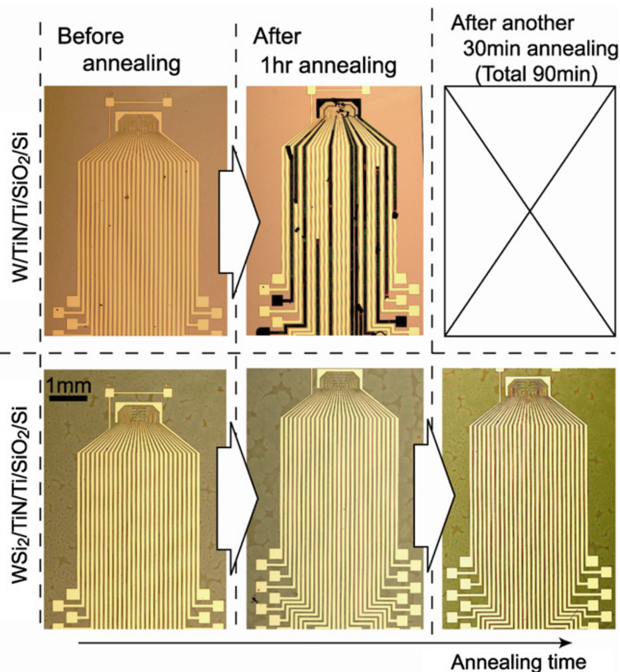

Figure 6. Conditions of several interconnections before and after annealing at 900 °C: W/TiN/Ti structure was fractured after 1 h of annealing, WSi_2/TiN/Ti does not show damage and adhered well, even after high-temperature annealing for over 1 h.

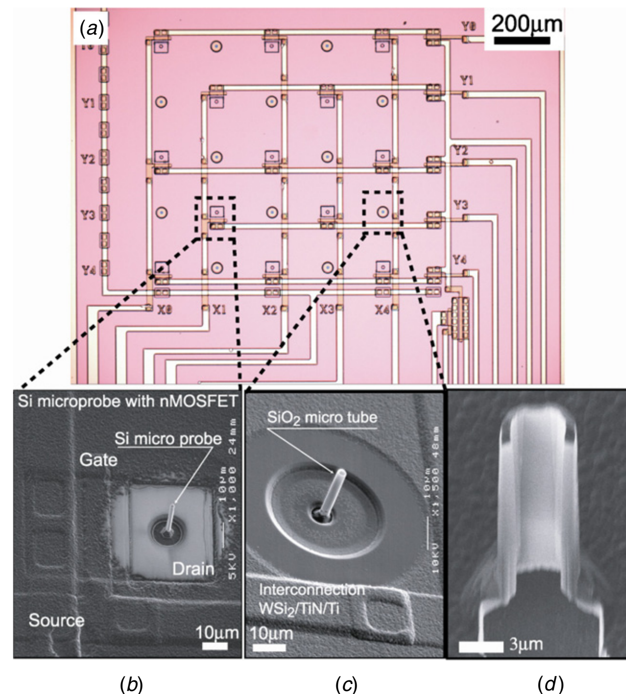

Figure 7. Images of fabricated device: (*a*) device photograph, (*b*) SEM image of a Si microprobe on the drain region of an NMOSFET, (*c*) SEM image of an on-chip tube structure (*b*) and (*d*) cross-sectional image of a fabricated microtube.

5.3. Influence of the post MOSFET processes and hydrogen annealing

Figure 8 shows the results of the drain current I_D- gate voltage V_{GS} characteristics of the on-chip NMOSFET. The dotted line depicts the condition prior to VLS growth. The subthreshold swing (S factor) and the leakage current of the MOSFET were 350 mV decade^{-1} and less than 10^{-11} A, respectively, while the threshold voltage was 1.6 V. However, after VLS growth and additional fabrication processes of the SiO_2 tube, the electrical properties of the MOSFET changed to 640 mV decade^{-1} for the S factor, 10^{-9} A for the leakage current and 2.8 V for the threshold voltage (dashed line in figure 8). Thus, it is hypothesized that the dangling bonds and interface states at the gate region of the MOSFET may be increased by the VLS growth and tube fabrication process such as high-temperature annealing in a vacuum ambient and exposure of the substrate to the plasma ambient. To improve the MOSFET property, hydrogen annealing for 3 h was conducted after entire process was completed, and significant changes were observed in the I_D–V_{GS} characteristics. The S factor decreased to 145 mV decade^{-1}, the leakage current was lowered to 10^{-12} A and the threshold voltage was reduced to 1.2 V. The reason for the changes in the electrical properties of the MOSFET after annealing is that the dangling bonds present at the interface between the gate oxide and the surface of the Si substrate are terminated with hydrogen atoms upon annealing [28]. Moreover, the characteristics after annealing were inferior to those of similar NMOSFETs on Si(1 0 0) substrate without extra processing such as the VLS growth and microfabrication process (S factor = 141 mV decade^{-1}, leakage current = 10^{-12} A). Hence, hydrogen annealing is an effective process for the device, regardless if VLS growth, phosphorous diffusion at 900 °C and tube fabrication processes had been performed. The results indicate that the device successfully integrated probes, tubes and on-chip MOSFETs.

5.4. Probe impedance and signal detection

Figure 9 shows the impedance of the Si microprobe as a function of frequency. Signals of neural spike appeared around 1 kHz. The probe impedance was approximately 2 MΩ at 1 kHz. Signal detection through the probe was also

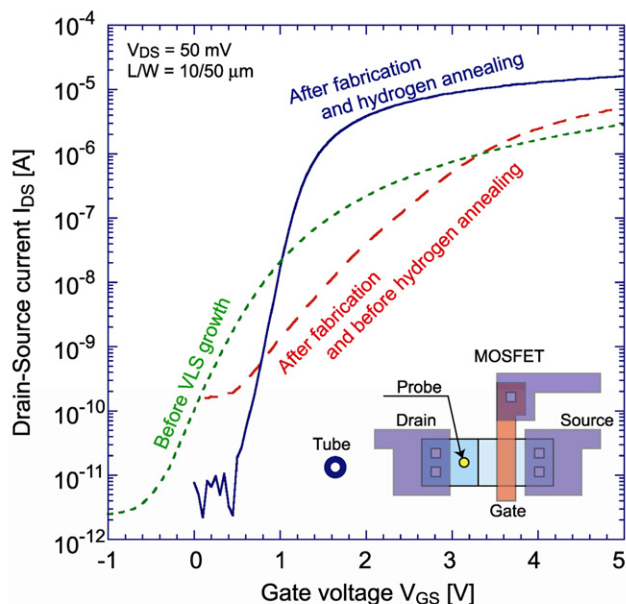

Figure 8. I_{DS}–V_{GS} curves of a fabricated NMOSFET on Si (1 1 1) before and after VLS growth and probe-tube processes: the dotted line is for before VLS growth and hydrogen annealing, the dashed line represents the fabrication process without hydrogen annealing, while the solid line indicates the result after hydrogen annealing for 3 h.

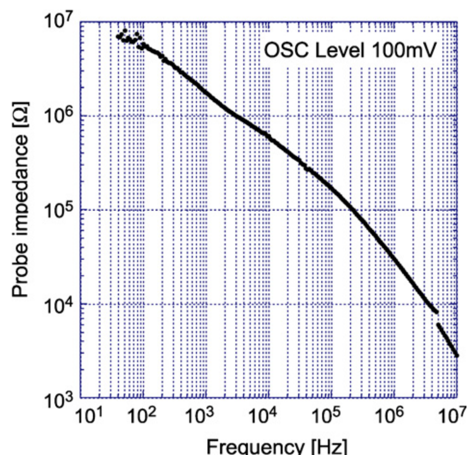

Figure 9. Probe impedance characteristic as a function of frequency.

investigated using a saline solution with input sinusoidal waves (80 $\mu V_{p\text{-}p}$ amplitude, 1 kHz). Figure 10 shows the obtained output signals through the probe, indicating a reduced amplitude of 45 $\mu V_{p\text{-}p}$. The noise level was about 20 $\mu V_{p\text{-}p}$.

The output/input signal ratio was 57%. We believe the reduced output signal is due to the parasitic capacitances that exist in the substrate (e.g. capacitors between the interconnections and the substrate at p–n junctions) and at the interface between the microprobe and the saline solution [29]. Hence, to improve the signal output/input ratio, the probe impedance and parasitic capacitances must be reduced.

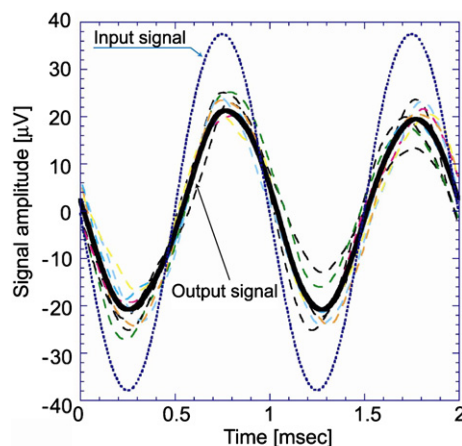

Figure 10. Output signals through the microprobe: dashed lines are the recording data and the solid line is the signal averaging data calculated from ten recordings. The amplitude of the input signal is 80 μV, and the output signal is 45 μV; the output/input signal ratio is 57%.

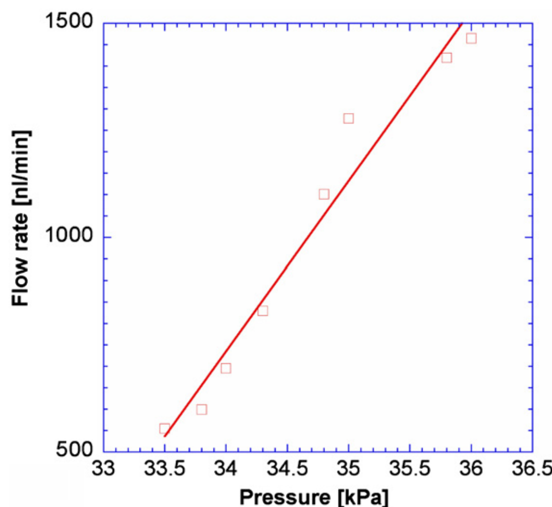

Figure 11. DI water flow rate through a single microtube as a function of flow pressure.

Moreover, on-chip amplifier circuitry may also improve the output/input signal ratio [26].

5.5. *Characteristics of liquid flow through the tube*

Figure 11 shows the flow characteristics of DI water through a single microtube with a length of 22 μm, and inner and outer diameters of 4.1 μm and 5.1 μm, respectively. Linear pressure-flow rate characteristics of the tube were experimentally measured and indicated that the flow amount of liquid can be varied using different flow pressures. The flow rate gradient, which depends on the flow pressure, was about 397 nl min^{-1} kPa^{-1}. According to our results, it is possible to control small amount of the liquid using the injection pressure and time. For example, an injection pressure of 33.5 kPa with an injection time of 2 min should provide 1 μl of a drug. In addition, investigations of drug-induced local neural responses

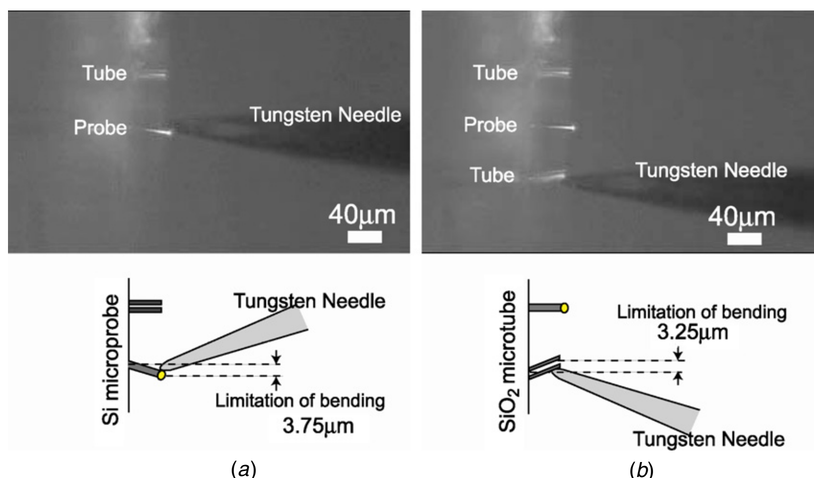

Figure 12. Microscope and schematic images of bending of a probe and a tube before being broken by a manipulated tungsten needle: to record the maximum displacement of (*a*) Si microprobe and (*b*) SiO_2 microtube.

may be plausible because the tube can control dosing in the nanoliter range flow rate.

5.6. Mechanical strength as a penetrating device

Maximum displacements of the tube (4 μm outer diameter, 40 μm height) and the probe (3 μm diameter, 42 μm height) were measured using a 5 μm diameter tungsten needle under a microscope. Figure 12 shows images from the bending tests for both the tube and the probe. The approximate maximum deflections of the tube and the probe were 3.3 μm and 3.8 μm, respectively. The bending experiment was repeated twice for each structure, and each deflection error was a few%

In the FEM simulation, the breakdown force at the tips of the tube and the probe, and the fracture stress at the bottom of them were calculated as functions of measured displacements. The calculation parameters used by the FEM are Young's moduli of 72 GPa and 188 GPa for SiO_2 and Si, respectively, and Poisson ratios of 0.14 and 0.177 for SiO_2 and Si, respectively. Figure 13 shows the analysis results. From both the experimental and simulation results, the microtube and the microprobe can withstand a force of about 380 μN and 87 μN, respectively (figures 13(*a*) and (*b*)). Moreover, the breakdown stress of the tube and the probe were 1.8 GPa and 2.8 GPa, respectively (figures 13(*a*) and (*b*)).

Figure 14 shows the result of device penetration into a gelatin, which was used to confirm the mechanical capabilities for the penetration devices. Figure 14(*a*) depicts the experiment prior to penetration. Figure 14(*b*) depicts the tube and probe array being inserted into the gelatin. After complete penetration, the gelatin was extracted from the tube and probe array as indicated in figure 14(*c*). These images show that the microtube and microprobe array can easily be inserted without breaking or causing the damage.

According to the mechanical experiment results, the tube and probe array has sufficient mechanical strength to penetrate into tissues. However, the arrays must be inserted perpendicular to the tissue because the array cannot withstand

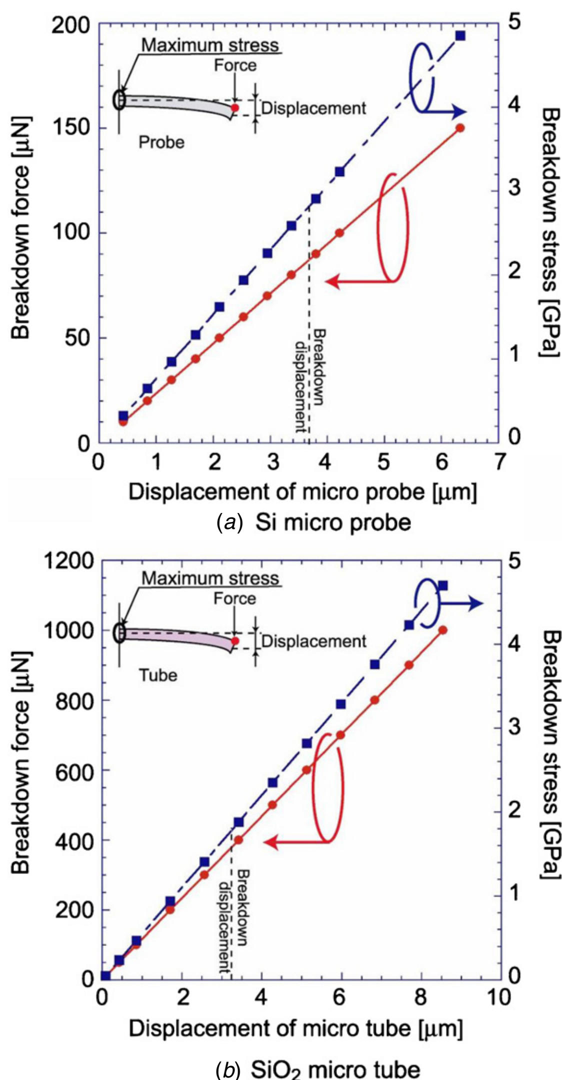

Figure 13. FEM simulation results of breakdown force and stress: (*a*) Si microprobe and (*b*) SiO_2 microtube.

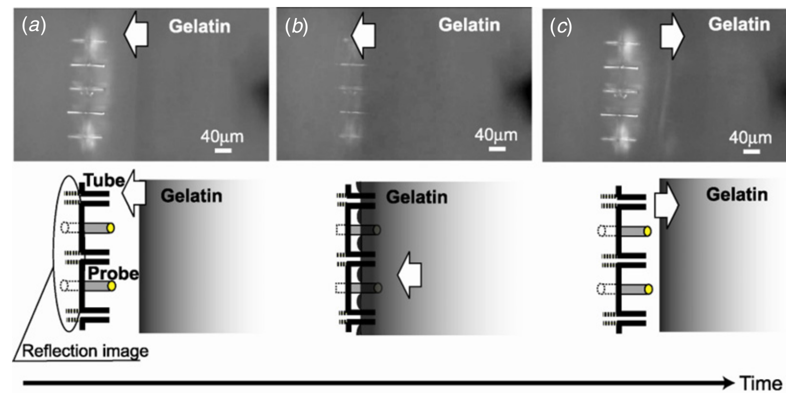

Figure 14. Photographs and schematic images of the probe and tube arrays inserted into gelatin: (*a*) before inserting into the gelatin, (*b*) during insertion and (*c*) extraction from the gelatin.

bending forces, which cause 3 to 4 μm displacement for a 40μm long tube/probe.

6. Conclusion

This paper reports a novel fabrication method, which achieves SiO_2 microtube and Si microprobe arrays integrated with circuits, using VLS growth and microfabrication processes. The fabricated tubes and probes have very fine tips, which are a few micron-meters and are minimally invasive to tissue during penetration. To incorporate the tube/probe with a circuit, interconnection materials and structures were considered, and based on our results a WSi_2/TiN/Ti structure was selected. The interconnection exhibited good adhesion, although the devices were exposed to a high-temperature ambient. In addition, the NMOSFET I_{DS}–V_{GS} characteristics after the tube and probe fabrication processes were measured. The properties were nearly the same as the standard MOSFET fabricated on the Si (1 0 0) substrate. Furthermore, the electrical properties of the Si microprobe and characteristics of liquid flow through a SiO_2 microtube were measured. The results indicate that the tube and probe array had sufficient mechanical capabilities to penetrate neuronal tissues.

In future, neural interface devices incorporating tubes, probes and signal processing circuits, can be realized using the proposed fabrication method. Herein, we report only a platform for the integration of tube and probe arrays with on-chip MOSFETs. Although the fabricated microtube and microprobe lengths are short to be used in penetrating applications, a longer VLS growth time can yield a tube/probe with a length in excess of 500 μm, and these longer tube/probes may be applicable as efficient neural interface devices in various neuroscience applications.

Acknowledgments

The authors would like to thank Mr Mitsuaki Ashiki for his assistance during the fabrication processes. Additionally, this work was supported by a grant-in-aid for Scientific Research (A)(MI), for JSPS fellows (KT), and the Global COE program 'Frontiers of Intelligent Sensing' from the Ministry of Education, Culture, Sports, Science and Technology of Japan (MI).

References

[1] Bear M F, Connors B W and Paradiso M A 2001 *Neuroscience Exploring the Brain* 2nd edn (Lippincott Williams & Wilkins Press: 22–675

[2] Chapin J K, Moxon K A, Markowitz R S and Nicolelis M A 1999 Real-time control of a robot arm using simultaneously recorded neurons in the motor cortex *Nat. Neurosci.* **2** 664–70

[3] Schaffer C B, Friedman B, Nishimura N, Schroeder L F, Tsai P S, Ebner F F, Lyden P D and Kleinfeld D 2006 Two-photon imaging of cortical surface microvessels reveals a robust redistribution in blood flow after vascular occlusion *PLOS Biol.* **4** 258–70

[4] Donoghue J P 2002 Connective cortex to machines: recent advances in brain interfaces *Nat. Neurosci.* **5** 1085–8

[5] Heuschkel M O, Fejtl M, Raggenbass M, Bertrand D and Renaud P 2002 A three-dimensional multi-electrode array for multi-site stimulation and recording in acute brain slices *J. Neurosci. Methods* **114** 135–48

[6] Branner A, Stein R B, Fernandez E, Aoyagi Y and Normann R A 2004 Long-term stimulation and recording with a penetrating microelectrode array in cat sciatic nerve *IEEE Trans. Biomed. Eng.* **51** 146–57

[7] Muthuswamy J, Okandan M, Jain T and Gilleti A 2005 Electrostatic microactuators for precise positioning of neural microelectrodes *IEEE Trans. Biomed. Eng.* **52** 1748–55

[8] Wise K D, Anderson D J, Hetke J F, Kipke D R and Najafi K 2004 Wireless implantable microsystems: high-density electronic interfaces to the nervous system *Proc. IEEE* **92** 76–97

[9] Parker E R, Rao M P, Turner K L, Meinhart C D and MacDonald N C 2007 Bulk micromachined titanium microneedles *J. Microelectromech. Syst.* **16** 289–95

[10] Stoeber B and Liepmann D 2005 Arrays of hollow out-of-plane microneedles for drug delivery *J. Microelectromech. Syst.* **14** 472–9

[11] Gardeniers H J G E, Luttge R, Berenschot E J W, de Boer M J, Yeshurun S Y, Hefetz M, van't Oever R and van den Berg A 2003 Silicon micromachined hollow microneedles for

transdermal liquid transport *J. Microelectromech. Syst.* **12** 855–62

[12] Griss P and Stemme G 2003 Side-opened out-of-plane microneedles for microfluidic transdermal liquid transfer *J. Microelectromech. Syst.* **12** 296–301

[13] Rajaraman S, Choi S-O, Shafer R H, Ross J D, Vukasinovic J, Choi Y, DeWeerth S P, Glezer A and Allen M G 2007 Microfabrication technologies for a coupled three-dimensional microelectrode, microfluidic array *J. Micromech. Microeng.* **17** 163–71

[14] Papageorgiou D P, Shore S E, Bledsoe S C and Wise K D 2006 A shuttered neural probe with on-chip flowmeters for chronic *in vivo* drug delivery *J. Microelectromech. Syst.* **15** 1025–33

[15] Ziegler D, Suzuki T and Takeuchi S 2006 Fabrication of flexible neural probes with built-in microfluidic channels by thermal bonding of parylene *J. Microelectromech. Syst.* **15** 1477–82

[16] Huang H and Fu C 2007 Different fabrication methods of out-of-plane polymer hollow needle arrays and their variations *J. Micromech. Microeng.* **17** 393–402

[17] Han M, Hyun D, Park H, Lee S S, Kim C and Kim C 2007 A novel fabrication process for out-of-plane microneedle sheets of biocompatible polymer *J. Micromech. Microeng.* **17** 1184–91

[18] Luttge R, Berenschot E J W, de Boer M J, Altpeter D M, Vrouwe E X, van den Berg A and Elwenspoek M 2007 Integrated lithographic molding for microneedle-based devices *J. Microelectromech. Syst.* **16** 872–84

[19] Yao Y, Gulari M N, Wiler J A and Wise K D 2007 a microassembled low-profile three-dimensional microelectrode array for neural prosthesis applications *J. Microelectromech. Syst.* **16** 977–88

[20] Hochberg L R, Serruya M D, Friehs G M, Mukand J A, Saleh M, Caplan A H, Branner A, Chen D, Penn R D and Donoghue J P 2006 Neuronal ensemble control of prosthetic devices by a human with tetraplegia *Nature* **442** 164–71

[21] Ishida M, Sogawa K, Ishikawa A and Fujii M 1999 Selective growth of Si wires for intelligent nerve potential sensors using vapor–liquid–solid growth *Proc. Int. Conf. Solid-State Sensors Actuators* pp 866–9

[22] Kawano T, Kato Y, Futagawa M, Takao H, Sawada K and Ishida M 2002 Fabrication and properties of ultrasmall Si wire arrays with circuits by vapor–liquid–solid growth *Sensors Actuators* A **97–8** 709–15

[23] Kawano T, Kato Y, Tani R, Takao H, Sawada K and Ishida M 2004 Selective vapor–liquid–solid epitaxial growth of micro-Si probe electrode arrays with on-chip MOSFETs on Si(1 1 1) substrates *IEEE Trans. Electron Dev.* **51** 415–20

[24] Kawano T, Ishihara A, Harimoto T, Takao H, Sawada K, Usui S and Ishida M 2004 Three-dimensional multichannel Si microprobe electrode array chip for analysis of the nervous system *Proc. Int. Electron Devices Meeting (IEDM 2004)* pp 1013–6

[25] Takei K, Kawashima T, Sawada K and Ishida M 2008 Out-of-plane micro tube arrays for biomedical sensors using vapor–liquid–solid growth method *IEEE Sensors J.* in press

[26] Sodagar A M, Wise K D and Najafi K 2007 A fully integrated mixed-signal neural processor for implantable multichannel cortical recording *IEEE Trans. Biomed. Eng.* **54** 1075–88

[27] Ghovanloo M and Najafi K 2007 A wireless implantable multichannel microstimulating system-on-a-chip with modular architecture *IEEE Trans. Neural Syst. Rehabil. Eng.* **15** 449–57

[28] Kato Y, Takao H, Sawada K and Ishida M 2004 The characteristic improvement of Si(1 1 1) metal-oxide–semiconductor field-effect transistor by long-time hydrogen annealing *Japan. J. Appl. Phys.* **43** 6848–53

[29] Robinson D A 1968 The Electrical properties of metal microelectrodes *Proc. IEEE* **56** 1065–71